The Journal of Neuroscience, June 1, 1996, 16(11):3549–3558

Multiple Structural Elements Determine Subunit Specificity of Mg^{2+} Block in NMDA Receptor Channels

Thomas Kuner[1] and Ralf Schoepfer[1,2]

[1]*Zentrum für Molekulare Biologie der Universität Heidelberg, Im Neuenheimer Feld 282, 69120 Heidelberg, Germany, and* [2]*University College London, Laboratory for Molecular Pharmacology, London WC1E 6BT*

In NMDA receptor channels, subtype-specific differences of Mg^{2+} block are determined by the NR2 subunits. Channels assembled from the NR1-NR2A or NR1-NR2B subunits are blocked more strongly than channels formed by the NR1-NR2C or NR1-NR2D subunits, predominantly reflecting a difference in voltage dependence. A determinant of Mg^{2+} block common to the NR2 subunits is located in the M2 domain (*N-site* or *Q/R/N-site*). However, subunit-specific differences of block suggested that additional structural elements exist. Chimeric NR2 subunits were constructed by replacing segments of the least sensitive NR2C subunit with homologous segments of the most sensitive NR2B subunit. Mutant NR2 subunits were coexpressed with wild-type NR1 in *Xenopus* oocytes, and Mg^{2+} block was quantified. Replacement of the entire M1–M4 region resulted in a chimera with a sensitivity of Mg^{2+} block similar to that of the NR2B wild type. Replacing smaller segments or introducing point mutations did not generate channels with Mg^{2+} block characteristic of NR2B wild type. However, combining in a single chimera three small segments (M1, M2–M3 linker, M4), each independently mediating an increase in Mg^{2+} block, produced channels close to NR2B wild type. Thus, differences in Mg^{2+} block as controlled by the NR2 subunits cannot be explained by a single structural determinant in addition to the *N-site*. Moreover, three elements of the NR2 subunit are the major determinants of subtype-specific differences of Mg^{2+} block in heteromeric NMDA receptor channels.

Key words: NMDA; receptor; channel; structure; recombinant; Mg^{2+} block; voltage dependence; subunit-specific

NMDA receptor (NMDAR) channels, composed from a common NR1 subunit (Moriyoshi et al., 1991; Yamazaki et al., 1992) and one or more of four different NR2 (A–D) subunits (Ikeda et al., 1992; Kutsuwada et al., 1992; Meguro et al., 1992; Monyer et al., 1992; Ishii et al., 1993), are thought to play a critical role in synaptic plasticity (Collingridge and Singer, 1990; Bliss and Collingridge, 1993), development of functional neuronal networks (Constantine, 1990; Shatz, 1990; Komuro and Rakic, 1993), and neuronal cell death (Choi, 1988). The NR1 subunit is expressed ubiquitously in the brain, whereas the NR2 subunits show a distinct spatial and temporal expression pattern (Watanabe et al., 1992; Akazawa et al., 1994; Monyer et al., 1994), thereby generating functional diversity of the NMDAR channel. For example, heterologously expressed NMDAR channels assembled from the NR1 and any one of the NR2 subunits, show NR2-specific differences in macroscopic kinetic properties (Monyer et al., 1992, 1994), single-channel characteristics (Stern et al., 1992), fractional Ca^{2+} currents (Burnashev et al., 1995), and voltage-dependent Mg^{2+} block (Kutsuwada et al., 1992; Monyer et al., 1992, 1994; Ishii et al., 1993).

The functional activation of NMDAR channels is linked to the membrane potential by the voltage dependence of Mg^{2+} block (Mayer et al., 1984; Nowak et al., 1984), allowing these channels to sense coincidence of synaptic input (Bliss and Collingridge, 1993). Differences in the extent of block by Mg^{2+} as determined by the NR2 subunit could be an important mechanism to create synapses with different characteristics for coincidence detection. Indeed, regional differences of Mg^{2+} block and changes during development have been reported (Kato et al., 1991; Kleckner and Dingledine, 1991; Kato and Yoshimura, 1993; Nabekura et al., 1994; Momiyama et al., 1995).

A determinant of Mg^{2+} block in NMDAR channels is located in the M2 domain of the NR2 subunits (*N-site* or *Q/R/N-site*) (Burnashev et al., 1992; Mori et al., 1992; Sakurada et al., 1993). The *N-site* is part of an octapeptide, which is conserved within the NR2 subunits. Despite having this shared element, channels containing NR2A or NR2B are more sensitive to Mg^{2+} block compared with NR2C- or NR2D-containing channels (Monyer et al., 1994), suggesting that additional elements exist that determine subunit specificity (Burnashev et al., 1992; Hollmann and Heinemann, 1994; McBain and Mayer, 1994; Sather et al., 1994; Seeburg et al., 1995).

We investigated the presence of additional elements for blockade by Mg^{2+} other than the *N-site* in the NR2 subunits by constructing chimeras between the NR2B and NR2C subunits. Homologous regions of the most sensitive NR2B subunit were grafted into the least sensitive NR2C subunit. Receptor channels containing any of the chimeric or wild-type NR2 subunits together with the wild-type NR1 subunit were expressed in *Xenopus* oocytes and functionally analyzed using a two-microelectrode voltage-clamp system. Our results indicate that three structural elements are required to convert an NR2 subunit with a low sensitivity to an NR2 subunit with a high sensitivity of Mg^{2+} block.

Received Nov. 8, 1995; revised March 20, 1996; accepted March 26, 1996.

This work was supported by SFB Grant 317/B9 to Peter H. Seeburg. R.S. is a Senior Wellcome Trust Fellow. We thank Dr. Peter H. Seeburg for his interest and support and Dr. Lonnie P. Wollmuth for critical discussions and technical advice. We are grateful to Drs. David Colquhoun, Dirk Feldmeyer, and Georg Köhr for commenting on this manuscript. We thank Annette Herold for DNA sequencing, Ulla Amtmann for technical assistance, and Christine Beck and Nicole Bender for help with mutagenesis.

Correspondence should be addressed to Thomas Kuner at the above address.

MATERIALS AND METHODS

Expression plasmid constructs. The coding regions of the NR1 (1a splice form (Hollmann et al., 1993)) and the NR2 subunits (Monyer et al., 1992, 1994) were cloned into a pSP64T-derived vector optimized for expression in *Xenopus* oocytes (Kuner et al., 1993). Noncoding regions were removed, and silent mutations were introduced to facilitate mutagenesis. The resulting NR1-SP, NR2A-SP, NR2B-SP, NR2C-SP, and NR2D-SP clones were used for all further manipulations. All mutants were constructed in a truncated version of the NR2C subunit as published by Monyer et al. (1992) (here denoted as NR2CΔ, 943 AA, see Fig. 5). Amino acids (AA) are shown in the single-letter code. Mutants carrying one AA substitution are named as "subunit(wild-type AA)position in the mature protein)mutant AA)." Chimeras are named according to the putative transmembrane domain(s) or loop(s) that were transplanted within a given fragment (e.g., *M14* contains M1–M4, *L2* contains the loop connecting M2 and M3; see Fig. 3 for detailed definition; Fig. 5 shows a schematic diagram).

Construction of chimeras. All mutants were constructed by PCR-based methods (Ausubel et al., 1994). For the chimeras, a set of primers was designed in a way to produce a PCR fragment of the desired region of the donor subunit that additionally carried the required restriction sites for subcloning into the recipient subunit. In most cases, we used a four-primer strategy permitting the introduction of a unique silent restriction site into the middle part of a fragment. This newly introduced site could then be used to insert smaller fragments, likewise carrying an additional site. Reiteration of this process allowed the introduction of progressively smaller fragments. We chose a distribution of restriction sites that allowed for reshuffling of most chimeras. All constructs were sequenced over the entire length of the replaced fragment.

Heterologous expression of NMDAR channels. NR2 wild-type and chimeric subunits were expressed with the NR1 subunit at a ratio of approximately 1:1 in *Xenopus* oocytes. Capped cRNA was transcribed for each expression construct with SP6 RNA polymerase (80 U/μl, Promega, Madison, WI) and examined electrophoretically on a denaturating agarose gel. To determine the concentration of the RNA solution, the gel was stained with ethidium bromide, and the intensities of the bands were compared with a length standard of defined quantity (0.24–9.5 kb RNA Ladder, Gibco Life Technologies, Eggenstein, Germany). Appropriate dilutions were prepared (0.01–1 μg/μl) to achieve expression levels in the range of 0.5–2 μA at −50 mV. *Xenopus laevis* oocytes were manually dissected from the ovary and placed in OR2 medium (NaCl, 82.5 mM; KCl, 2.5 mM; Na_2HPO_4, 1 mM; HEPES, 5 mM; $MgCl_2$, 1 mM; $CaCl_2$, 1 mM; PVP, 0.5 gm/l, pH adjusted to 7.2 with NaOH) supplemented with penicillin and streptomycin (100 U/ml, Gibco). The oocytes were injected with 20–40 nl of RNA solution using a Nanoject injector (Drummond, Broomall, PA), incubated at 19°C, and treated with collagenase type II (1 mg/ml, Sigma, St. Louis, MO) after 12–24 hr of incubation. Whole-cell recordings were made at room temperature 3–8 d after injection of the oocytes.

Experimental protocol: quantification of Mg^{2+} block. All recordings were performed on a two-microelectrode voltage-clamp setup (TEC 01/2C, NPI Electronic, Tamm, Germany) modified for computer-controlled, automatic application of different solutions, voltage ramps, and data acquisition (custom made using LabVIEW, National Instruments, Austin, TX). Electrodes were pulled from borosilicate glass and filled with 3 M KCl. The resistance was kept in the range of 0.5–2 MΩ. Oocytes were clamped at −50 mV, and voltage ramps were applied (−120 to +20 mV, within 2 sec). Current records were filtered with a Bessel 4-pole low-pass filter at 30 Hz and digitized with a sampling rate of 100 Hz. The recording chamber had a volume of 200 μl and was continuously perfused at 1–2 ml/min. To minimize interactions of Mg^{2+} and Ca^{2+} (Mayer and Westbrook, 1987; Ascher and Nowak, 1988) and contamination by Ca^{2+}-activated Cl^- currents (Leonard and Kelso, 1990), all experiments were made in low Ca^{2+} Ringer's solution containing (in mM): 0.18 $CaCl_2$, 115 NaCl, 2.5 KCl, and 10 HEPES adjusted to pH 7.2 with NaOH.

The following protocol was used to obtain current–voltage (*I–V*) curves in the presence of different Mg^{2+} concentrations. First, the Mg^{2+} concentration to be tested was applied in the presence of glycine (10 μM) for 50–180 sec to obtain the leakage *I–V* curve. Then, the same solution, but in addition containing glutamate (100 μM), was applied for 40 sec, and a test *I–V* curve was recorded. Different Mg^{2+} concentrations were separated by a 3 min wash with low Ca^{2+} Ringer's. This type of experiment was executed in the sequence 0 μM (i.e., nominally Mg^{2+}-free solution), 1 μM, 10 μM, 100 μM, 1 mM, 0 μM Mg^{2+}. We refer to one such sequence as a series, and a set consisted of two-to-three consecutive series. Only sets with reasonably stable series were selected for further analysis.

Data were analyzed using Igor (WaveMetrics). Leakage *I–V* curves were subtracted from test *I–V* curves. Normalized *I–V* curves were calculated relative to the value at −100 mV of the nominally Mg^{2+}-free solution (Figs. 1, 4). For each Mg^{2+} concentration, the fractional block at −100 mV was determined. Data derived from individual series of a set were averaged. The $IC_{50,-100mV}$ of a set was obtained by fitting the averaged data points with the function:

$$y = \frac{100}{1 + \left(\frac{[Mg^{2+}]}{IC_{50}}\right)^{n_H}}, \quad (1)$$

where y is percentage of control current at a given membrane potential, 100 is maximal current in nominally Mg^{2+}-free solution, $[Mg^{2+}]$ is the concentration of extracellular Mg^{2+}, n_H is the Hill coefficient, and IC_{50} is half-maximal block by Mg^{2+}.

Quantification of voltage dependence. Voltage dependence of block (δ, fraction of the electric field that the blocker experiences) and affinity of Mg^{2+} at 0 mV [$K_{0.5}(0)$] were calculated by determining the IC_{50} (Eq. 1) at different potentials (−25 to −115 mV, increments of 5 mV). The logarithm of the resulting IC_{50} values was plotted against the holding potential, and a straight line was fitted to the data points over a voltage range from −80 to −30 mV. The apparent δ and $K_{0.5}(0)$ were then calculated according to Woodhull (1973):

$$K_{0.5}(V) = K_{0.5}(0) \times \exp\left(\frac{z\delta VF}{RT}\right), \quad (2)$$

where z is valence, V is membrane potential, and R, T, and F have their usual meaning.

Statistical analysis. The logarithm of the IC_{50} values was used to calculate the mean, SEM, and one-way ANOVA. Significance levels were assessed with the Tukey–Kramer test using the GB-STAT software (Dynamic Microsystems, Silver Spring, MD).

RESULTS

Mg^{2+} block of wild-type NMDAR channels expressed in *Xenopus* oocytes

NMDAR channels assembled from the constitutive NR1 and any one of the four NR2 subunits (A,B,C,D) were differently blocked by Mg^{2+} (Fig. 1). Channels containing the NR2A or NR2B subunit were more strongly blocked compared with channels containing NR2C or NR2D. In the presence of 1 mM Mg^{2+}, the NR2A- or NR2B-containing channels were almost completely blocked at −100 mV and passed maximal current at approximately −25 mV. In contrast, NR2C- or NR2D-containing channels were incompletely blocked at −100 mV and passed maximal current at a less depolarized potential of approximately −35 mV (Fig. 1). In all experiments reported here, current responses were nondesensitizing given the time resolution of our system (not shown). To quantify Mg^{2+} block, we determined the concentration of Mg^{2+} for half-maximal block at −100 mV ($IC_{50,-100mV}$, see Materials and Methods). Dose–response curves for Mg^{2+} block of individual records of NR1-NR2C and NR1-NR2B channels are illustrated in Figure 2, *A* and *B* (shown as the *thick line*). Averaged $IC_{50,-100mV}$ values are listed in Table 1 and shown graphically in Figure 5.

The normalized *I–V* curves shown in Figure 1 suggest a different voltage dependence of block between channels containing NR2A or NR2B versus channels containing the NR2C or NR2D. Voltage dependence was analyzed according to the Woodhull model (see Materials and Methods). Figure 2, *A* and *B*, shows dose–response curves at selected potentials derived from the records displayed in Figure 1. The logarithm of IC_{50} values obtained at different potentials was plotted against the holding potential, and a straight line was fitted to determine δ

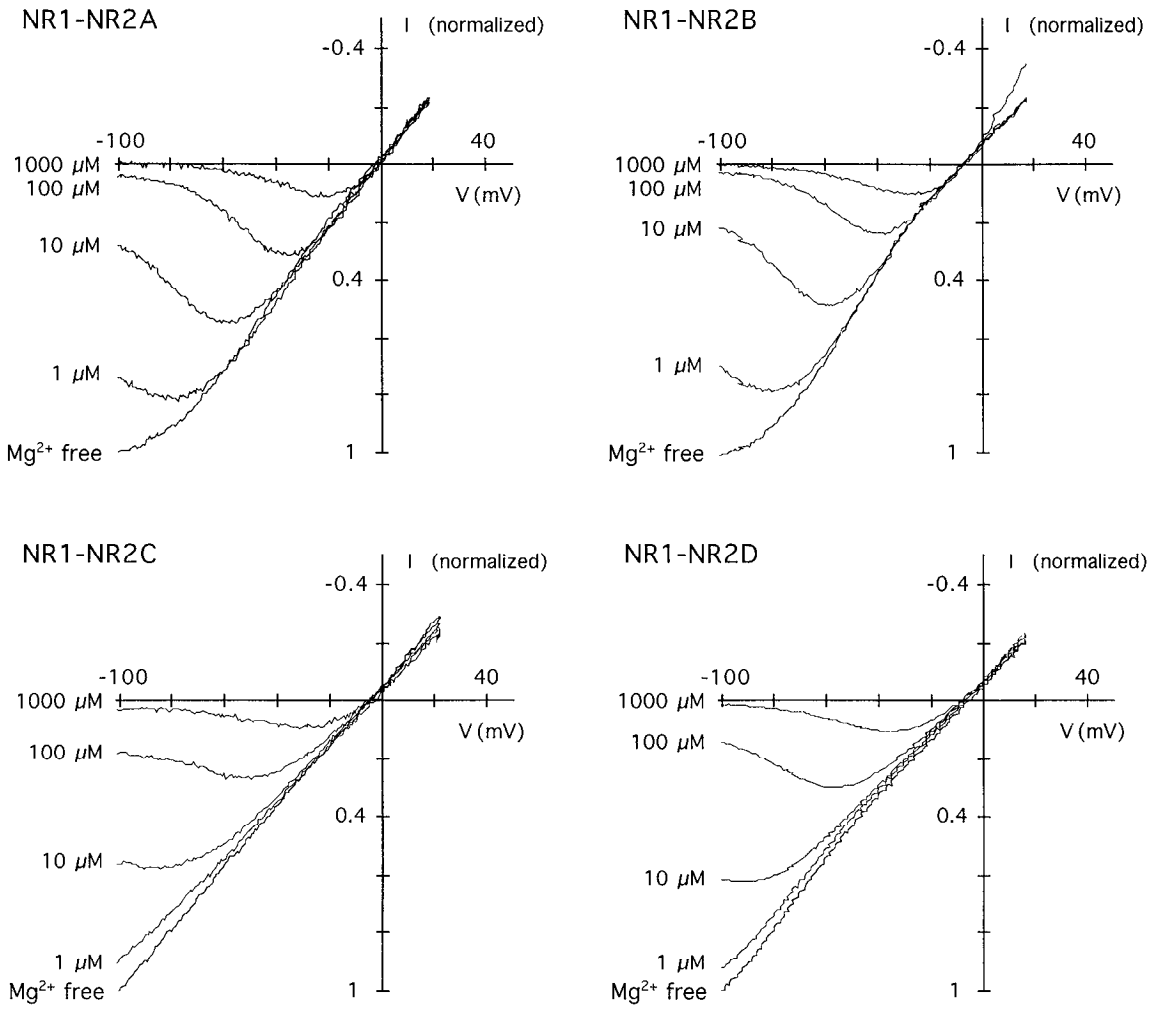

Figure 1. Differential Mg^{2+} block of four NR1-NR2 subtypes expressed in *Xenopus* oocytes. Representative *I–V* curves recorded in the presence of different Mg^{2+} concentrations in low Ca^{2+} Ringer's. *I–V* curves were normalized to the current at −100 mV in nominally Mg^{2+}-free solution. $IC_{50,-100mV}$ values are shown in Table 1. The control *I–V* curves of NR1-NR2A and NR1-NR2B were slightly blocked by residual Mg^{2+} in the Ringer's. However, the influence on calculation of the $IC_{50,-100mV}$ was negligible, and the values given in Table 1 might be slight underestimates of the true $IC_{50,-100mV}$. Variations of the reversal potential in the range of −10 to 0 mV were observed between different oocytes. In some instances, the outward current passed by NR1-NR2B channels was potentiated in the presence of 1 mM Mg^{2+}.

and $K_{0.5}(0)$. Individual examples for each subtype are shown in Figure 2*C*. A deviation from the linear relation predicted by the Woodhull expression was observed. The deviation was most pronounced at very negative potentials and more prominent in NR1-NR2A and NR1-NR2B channels compared with NR1-NR2C and NR1-NR2D channels. This nonlinearity constituted the problem of finding the appropriate voltage range to fit the data. At potentials more negative than −90 mV, the deviation from linearity was too strong (Fig. 2*C*), whereas at potentials more positive than −30 mV, the error in calculating IC_{50} values was too large. Within these borders, the most accurate fits were found in the range of −80 to −30 mV, which was then taken to determine δ and $K_{0.5}(0)$. NR2A- or NR2B-containing channels displayed a higher voltage dependence ($\delta \sim 1$) compared with channels containing NR2C or NR2D ($\delta \sim 0.7$). The four subtypes were not significantly different regarding $K_{0.5}(0)$ (Table 1). Because $K_{0.5}(0)$ showed a considerable variability, we applied two additional approaches (DiFrancesco et al., 1982; Ruppersberg et al., 1994) to analyze voltage dependence of the four subtypes. Both methods yielded similar results and a comparable degree of variability (not shown).

Chimeric NR2 subunits: construction and functional analysis

Chimeric NR2 subunits were generated by replacing fragments of the least sensitive NR2C subunit with homologous fragments of the most sensitive NR2B subunit (Fig. 3; Fig. 5, *left panel*). As the recipient NR2C subunit, a truncated version lacking the C-terminal 275 amino acids (NR2CΔ, see Materials and Methods) was used. When coexpressed with the NR1 subunit, the resulting channel showed no differences in Mg^{2+} block (Table 1, Fig. 5) or single-channel characteristics (Schoepfer et al., 1994) compared with channels containing the full-length NR2C subunit.

Comparison of the amino acid sequence between the core regions (M1–M4) of the NR2 subunits shows a high overall sequence similarity (Fig. 3). The hydrophobic domains (especially M3) appear to be more conserved than, for example, the L3 loop (for nomenclature, see Fig. 5, *left panel*) or the region following M4. Also, the stretch of amino acids preceding M1, a region involved in agonist binding (Stern-Bach et al., 1994), exhibits almost 100% sequence identity. In addition, the alignment reveals that group-specific differences (at homologous positions: [NR2A

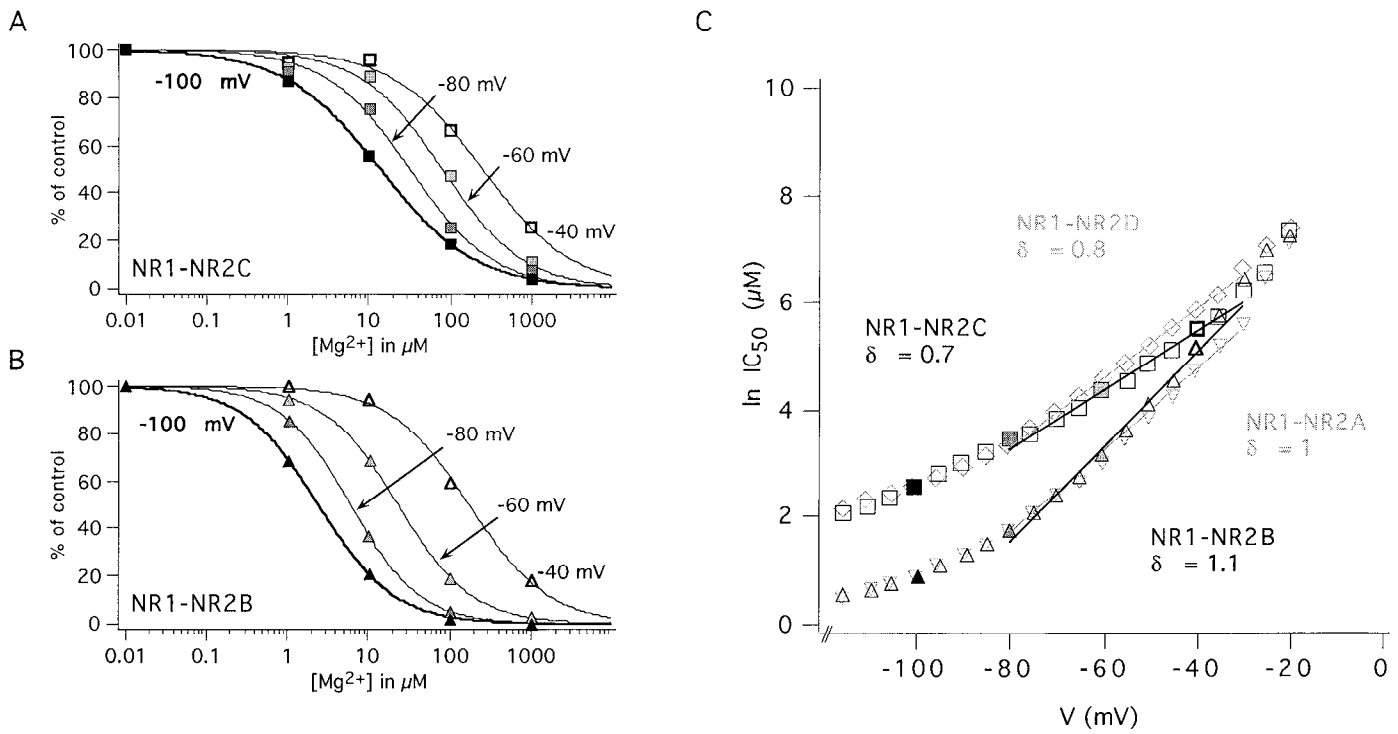

Figure 2. Voltage dependence of Mg^{2+} block. *A*, Dose–response curves for Mg^{2+} at different potentials (−100, −80, −60, −40 mV) derived from the *I–V* curve of NR1-NR2C shown in Figure 1. Values of the fractional block are shown as *squares*. The fit used to determine the $IC_{50,-100mV}$ (in this example, 14.7 μM Mg^{2+}) is shown as a *thick line*. *B*, Same as in *A* for NR1-NR2B; values of the fractional block derived from the *I–V* curve shown in Figure 1 are shown as *triangles*. The $IC_{50,-100mV}$ is 2.4 μM Mg^{2+}. *C*, Difference in voltage dependence of the two representative Mg^{2+} series shown in *A* and *B* and Figure 1 (printed in *black*). The data were fitted in the range from −80 to −30 mV, as indicated by the two lines. Examples for the NR1-NR2A and NR1-NR2D are printed in *gray*.

= NR2B] ≠ [NR2C = NR2D], *underlined*) occur more frequently within the hydrophobic domains compared with other areas (e.g., L1 loop, L3 loop, or C-terminal of M4).

All chimeras were coexpressed with the NR1 subunit and generated whole-cell currents comparable to wild type (Table 1). Chimeras were analyzed as described for the wild-type subunits; first we present results based on the analysis of half-maximal block, then we describe voltage dependence of Mg^{2+} block.

Influence of the M2 domain on subunit specificity of Mg^{2+} block

In the close vicinity of the *N-site* within the M2 domain, few amino acid positions differ between the subunits (Fig. 3). We created an M2 domain similar to NR2B by substituting three amino acids (SV..A to AI..G, see Fig. 3) on the N-terminal side of the *N-site* in the NR2C. The resulting NR2C-M2a chimera could not be distinguished functionally from NR2C wild type (Fig. 5, Table 1). On the C-terminal side of the *N-site* at the border of M2 (Fig. 3), two positions differ between NR2B and NR2C. When mutated individually, the $IC_{50,-100mV}$ of both NR2C(I598V)- and NR2C(E599Q)-containing channels was close to wild-type NR2C (Table 1).

Contribution of the M1–M4 segment

Because replacement of residues within M2 of NR2C was without effect on Mg^{2+} block, we investigated regions adjacent to the M2 domain. In a first attempt, the M1–M3 region was transferred from the NR2B into the NR2C subunit to yield NR2C-M13 [Fig. $3^{A/E}$ (the letters in superscript refer to the segment exchanged between NR2B and NR2C)]. This chimera exhibited a strongly increased sensitivity of Mg^{2+} block compared with NR2C wild type (Fig. 4*A*, Table 1). However, Mg^{2+} block was not as sensitive as wild-type NR2A or NR2B (Fig. 5). In a second attempt, we transplanted the complete M1–M4 region of NR2B into NR2C, thereby creating chimera NR2C-M14 (Fig. $3^{A/I}$). Functional analysis of this chimera (Fig. 4*B*) revealed an $IC_{50,-100mV}$ indistinguishable from NR2A or NR2B wild type (Table 1, Fig. 5).

Identification of individual elements within the M1–M4 segment

In an attempt to detect single amino acid residues mediating the increase of Mg^{2+} block found in NR2C-M14, the M1–M4 segment was subdivided into smaller units (see Fig. 5, *left panel*). The difference in sensitivity to Mg^{2+} block between NR2C-M13 and NR2C-M14 suggested that the M3–M4 segment may contain a structural determinant, in addition to elements present in the M1–M3 segment. To test this idea, chimera NR2C-M34 was constructed (Fig. $3^{E/I}$). Functional analysis revealed a significant increase in sensitivity of Mg^{2+} block relative to NR2C wild type (Fig. 5, Table 1). However, this increase was less pronounced than determined for its N-terminal counterpart, NR2C-M13. Chimeras NR2C-M13 and NR2C-M34 were each subdivided to yield an N-terminal and a C-terminal set of chimeras.

Chimera NR2C-M13 was split into NR2C-M12 and NR2C-L2, the former containing M1 and M2 (Fig. $3^{A/D}$), the latter carrying the L2 linker between M2 and M3 (Fig. $3^{D/E}$). Chimera NR2C-M12 was less sensitive to Mg^{2+} block than NR2C-M13, but significantly more sensitive than NR2C wild type (Fig. 5, Table 1). A slightly higher sensitivity to Mg^{2+} block was found

Table 1. Whole-cell current expression, Mg^{2+} concentration for half-maximal block, and voltage dependence of wild-type and mutant channels

	Expression at −50 mV (nA)	Mg^{2+} $IC_{50,-100mV}$ (μM)*	n **	Mg^{2+} δ	Mg^{2+} $K_{0.5}(0)$ (mM)	n
NR2A	−2925 ± 2380	2.4 (1.5/4.0)	7	1.05 ± 0.06	4.8 ± 1.8	4
NR2B	−141 ± 64	2.1 (1.5/2.8)	7	1.07 ± 0.04	3.7 ± 1.1	4
NR2C	−690 ± 474	14.2 (11.1/16.5)	10	0.73 ± 0.03	3.5 ± 1.1	7
NR2D	−1160 ± 814	10.2 (8.5/12.4)	5	0.75 ± 0.02	2.6 ± 1.1	6
NR2CΔ	−650 ± 758	15.6 (13.5/17.9)	5	0.78 ± 0.04	4.9 ± 1.9	3
M1	−2580 ± 2099	9.4 (5.9/12.1)	5	0.92 ± 0.02	5.9 ± 1.3	5
M12	−663 ± 437	9.7 (7.2/13.9)	5	0.95 ± 0.02	10.2 ± 1.5	4
L1	−790 ± 498	13.2 (10.7/15.6)	4	0.71 ± 0.04	2.4 ± 0.4	3
M2a	−625 ± 204	15.2 (11.3/18.0)	6	0.72 ± 0.05	3.6 ± 0.8	5
L2	−2163 ± 1931	7.9 (6.4/9.6)	4	0.94 ± 0.04	5.3 ± 1.6	3
M13	−1571 ± 1191	4.8 (3.9/7.2)	5	0.86 ± 0.02	2.1 ± 0.3	3
M14	−538 ± 483	2.7 (2.3/3.4)	6	0.92 ± 0.04	1.9 ± 0.8	4
M34	−667 ± 153	7.6 (6.5/10.2)	5	0.85 ± 0.02	3.2 ± 0.3	3
M34a	−1375 ± 733	7.3 (6.0/8.7)	4	0.80 ± 0.06	2.8 ± 0.9	4
M4	−480 ± 208	9.0 (7.8/10.6)	4	0.87 ± 0.06	4.5 ± 1.1	4
M4a	−800 ± 510	9.3 (6.5/12.2)	6	0.87 ± 0.05	5.2 ± 2.4	4
M1L2M4a	−1020 ± 383	4.9 (3.3/5.8)	5	1.04 ± 0.02	8.1 ± 1.1	5
NR2C(I598V)	−1500 ± 791	13.2 (10.7/14.9)	4	0.92 ± 0.04	10.3 ± 2.8	4
NR2C(E599Q)	−616 ± 326	15.4 (10.0/19.9)	6	0.86 ± 0.10	9.8 ± 5.2	4
NR2C(R602K)	−950 ± 252	14.0 (10.1/16.1)	4	0.85 ± 0.04	6.6 ± 1.1	4
NR2C(L611S)	−1780 ± 421	14.1 (9.8/20.7)	5	0.98 ± 0.03	11.0 ± 1.9	3

*Averaged Hill coefficient n_H = 0.93 ± 0.01 (n = 112).

**Number of sets (for definition of a set, see Materials and Methods).

Expression is shown as mean ± SD; IC_{50} values are given as mean (min/max); δ and $K_{0.5}(0)$ are shown as mean ± SEM.

when chimera NR2C-L2 was examined (Figs. 4*C*, 5). Interestingly, this chimera introduced changes at only four amino acid positions, two of which were already shown to have no effect on the $IC_{50,-100mV}$ [NR2C(I598V) and NR2C(E599Q), see above]. The remaining two positions were mutated individually [NR2C(R602K) and NR2C(L611S), see Fig. 3]. Unexpectedly, none of these mutants differed significantly from wild-type NR2C with regard to the $IC_{50,-100mV}$ of Mg^{2+} block (Table 1). Chimera NR2C-M12 was divided into NR2C-M1, carrying M1 of NR2A (Fig. $3^{A/B}$) and NR2C-L1, containing the small heterogeneous L1 linker between M1 and M2 of NR2B (Fig. $3^{B/C}$). Mg^{2+} block of NR2C-M1 showed a similar sensitivity to that of NR2C-M12, but NR2C-L1 was indistinguishable from NR2C wild type (Fig. 5, Table 1).

Chimera NR2C-M34 was subdivided to yield NR2C-M34a, containing the C-terminal half of L3, the M4 domain, and a short stretch of the C terminus (Fig. $3^{F/I}$). NR2C-M34a exhibited a similar sensitivity to Mg^{2+} block than NR2C-M34 (Fig. 5). In a further step, the C-terminal half of this chimera was retained, thereby creating chimera NR2C-M4 (Fig. $3^{G/I}$). Sensitivity to Mg^{2+} block of NR2C-M4 was comparable to the effect found for NR2C-M34 (Fig. 5). To investigate whether the M4 domain or the heterogeneous part C-terminal to M4 contains the responsible determinant, we constructed chimera NR2C-M4a (Fig. $3^{G/H}$). This chimera exhibited the same sensitivity to Mg^{2+} block as NR2C-M4 (Fig. 5).

To summarize, three small elements within the M1–M4 segment independently mediated an increase in sensitivity to Mg^{2+} block. These elements are contained on chimeras NR2C-M1, NR2C-L2, and NR2C-M4a. Chimera NR2C-L2 was further analyzed for single amino acid determinants, but no attempt was made to identify single amino acid residues within the NR2C-M1 and NR2C-M4a chimeras.

Combination of the three elements M1, L2, and M4

Insertion of the M1–M4 region of the NR2B into the NR2C resulted in a channel with an NR2B-like phenotype of Mg^{2+} block. However, no single determinant could be detected within the M1–M4 region. We combined the three smallest elements that showed a significant effect by themselves in one single chimera, NR2C-M1L2M4a (Fig. $3^{A/B,D/E,G/H}$). Mg^{2+} block of the resulting channel was enhanced more than observed for any of the elements alone and was close, but not identical, to that of wild-type NR1-NR2B (Figs. 4*D*, 5, Table 1).

Voltage dependence of chimeric NR2 subunits

Analysis of the chimeras for voltage dependence of Mg^{2+} block revealed a pattern as expected from the $IC_{50,-100mV}$ values described above. Consistent with the observation that NMDAR wild-type channels differ in their δ but exhibit a similar $K_{0.5}(0)$, we found that the chimeras also differed in δ but were not statistically different with regard to the affinity of Mg^{2+} at 0 mV. Most of the chimeras displayed intermediate δ values and were not significantly different from either NR2B or NR2C wild types (Fig. 5, Table 1). Only the N-terminal mutants NR2C-M1, NR2C-M12, NR2C-L2, and NR2C(L611S) exhibited significantly increased voltage dependence compared with NR2C wild type. The NR2C-M1L2M4a chimera showed the strongest increase in voltage dependence and could not be distinguished from wild type NR2B (Fig. 5). The chimeras with the largest decrease in $IC_{50,-100mV}$, NR2C-M13 and NR2C-M14, exhibited an increase of δ, albeit not statistically significant. In contrast to the N-terminal chimeras, C-terminal chimeras showed no significant change in voltage dependence. $IC_{50,-100mV}$ values of all mutants could be calculated from pairs of averaged $K_{0.5}(0)$ and δ values given in Table 1 and presented with the same pattern as found for the measured $IC_{50,-100mV}$ values (not shown).

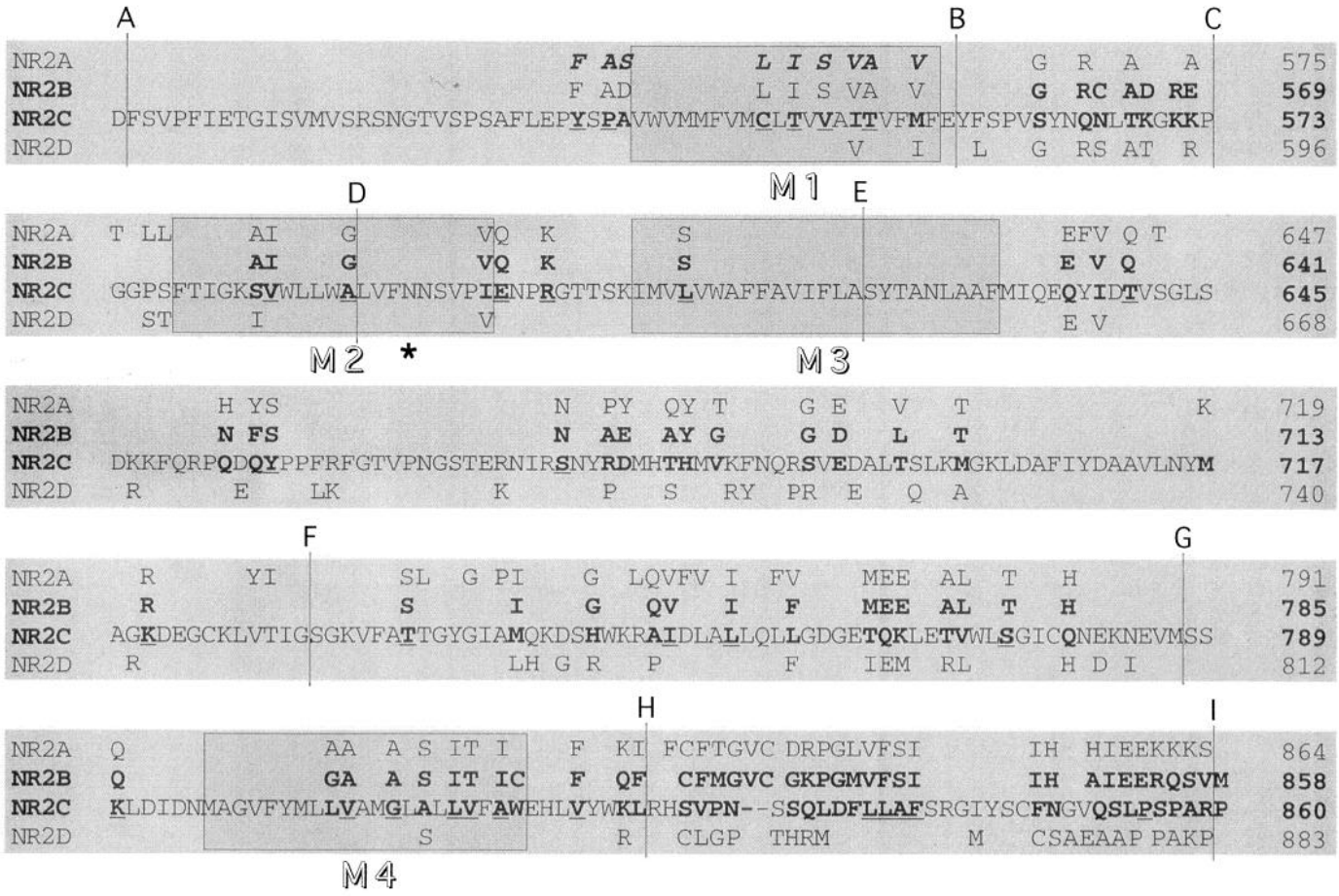

Figure 3. Alignment of the core region of rat NR2 subunit amino acid sequences including the four hydrophobic domains (M1–M4). An *asterisk* indicates the location of a determinant of Mg^{2+} block in the M2 domain (*N-site*). Residues printed in *boldface* were exchanged in a given chimera, and *underlined* positions emphasize group-specific differences ([NR2A = NR2B] ≠ [NR2C = NR2D]) in amino acid sequence. *Numbers* given on the *right* side indicate the position of the rightmost amino acid in each row (72 AA) within the given subunit. Fusion positions of chimeras are denoted by *capital letters* in the order of their appearance: *M1 = A/B* (only for this chimera, the sequence of NR2A was inserted, printed in *bold italic letters*); M12 = *A/D*; L1 = *B/C*; M13 = *A/E*; M2a = SV..A replaced by AI..G; L2 = *D/E*; M14 = *A/I*; M34 = *E/I*; M34a = *F/I*; M4 = *G/I*; M4a = *G/H*.

DISCUSSION

The present study revealed structural determinants for NR2 subunit-specific Mg^{2+} block in heteromeric NMDAR channels. As indicated by the work of Monyer et al. (1994), channels containing NR1 and any one of four NR2 subunits fall into two groups with regard to their sensitivity to external Mg^{2+} block. Receptor channels containing the NR2A or NR2B subunits are characterized by a higher sensitivity ($IC_{50,-100mV} \sim 2\ \mu M$), whereas channels containing NR2C or NR2D exhibit a lower sensitivity of Mg^{2+} block ($IC_{50,-100mV} \sim 10–15\ \mu M$). Differences of $IC_{50,-100mV}$ values shown here compared with IC_{50} values reported in other studies arise in part from calculation of the fractional block at potentials less negative than −100 mV (Kawajiri and Dingledine, 1993). In addition, differences may be attributable to the presence of millimolar concentrations of Ca^{2+} or Ba^{2+} (Ishii et al., 1993; Kawajiri and Dingledine, 1993) in the external solution. To reduce interaction between Ca^{2+} and Mg^{2+} (Mayer and Westbrook, 1987; Ascher and Nowak, 1988), Ringer's solution containing 0.18 mM Ca^{2+} was used in our study.

Analysis of voltage dependence in wild-type NMDAR channels

The Woodhull model of voltage-dependent block predicts a linear relationship between the $\ln(IC_{50,mV})$ of the blocker and the membrane potential. In contrast, we found a deviation from linearity toward a lower voltage dependence of Mg^{2+} block, consistent with the observations of Kleckner and Dingledine (1991). This deviation was most prominent at potentials more negative than −80 mV in all four subunits, but the more sensitive NR1-NR2A and NR1-NR2B channels deviated more strongly compared with the less sensitive NR1-NR2C and NR1-NR2D channels. The best approximation of a linear Woodhull relation was found in the range of −80 to −30 mV; therefore, this range was used to determine δ and $K_{0.5}(0)$. Two explanations for the inconsistencies between data and model may be relevant (Ascher and Nowak, 1988; Kleckner and Dingledine, 1991). First, Mg^{2+} might be a permeant blocker (Mayer and Westbrook, 1987). Second, Ca^{2+} attenuates Mg^{2+} block at hyperpolarized potentials (Mayer and Westbrook, 1987). These two actions may be additive and subunit-specific.

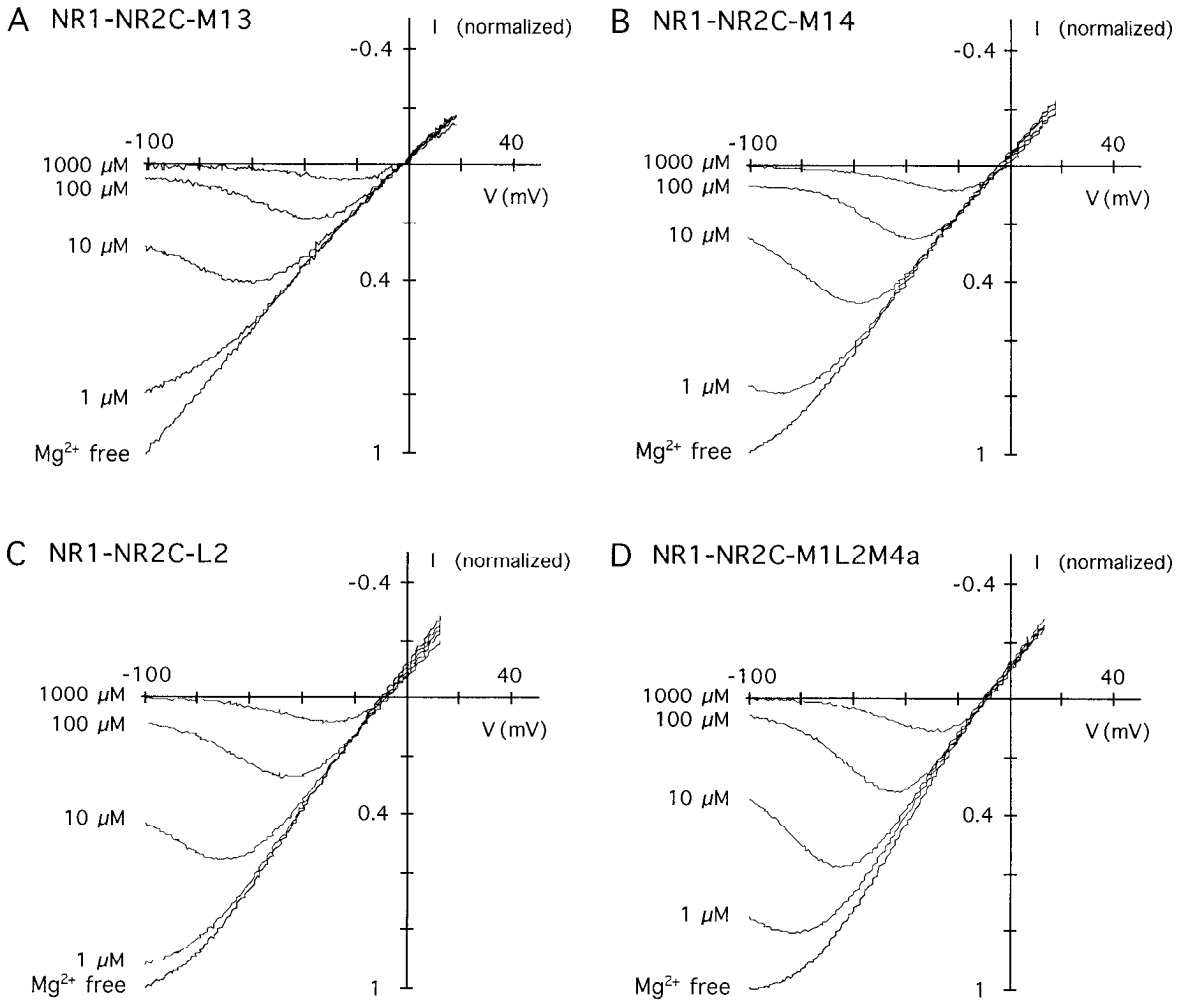

Figure 4. Selected *I–V* curves of four chimeras representing different levels of Mg^{2+} block. See also legend to Figure 1. $IC_{50,-100mV}$ values are shown in Table 1.

NMDAR channels containing the more sensitive NR2A or NR2B subunits show a higher voltage dependence ($\delta \sim 1$) compared with channels containing NR2C or NR2D ($\delta \sim 0.7$). However, both groups show a similar affinity for Mg^{2+} at 0 mV ($K_{0.5}(0) \sim 3.5$ mM). Our analysis of recombinant NMDAR channels revealed values that are in the range of previously published data obtained from native NMDAR channels. For example, δ and $K_{0.5}(0)$ values of 1 and 8.8 mM have been reported by Ascher and Nowak (1988), ~0.8 and 1.8 mM by Jahr and Stevens (1990), 0.73 and 1.1 mM by Chen and Huang (1992). Inspection of the data presented here, as well as comparison to data published by others, reveals that the values reported for δ are in good agreement, whereas the $K_{0.5}(0)$ values show a considerable variability. This might be related to a systematic error in quantification of $K_{0.5}(0)$, which in most methods is determined by extrapolation of a fit applied to a voltage range distant from 0 mV. Thus, small errors in fitting the data can create a large variability of $K_{0.5}(0)$. In conclusion, the four subtypes appear to be similar in binding given the sensitivity of our system, but small differences cannot be ruled out. Nevertheless, subunit-specific differences in Mg^{2+} block predominantly reflect a difference in voltage dependence (δ).

Structural elements mediating subunit specificity of Mg^{2+} block

Our data demonstrate that an NR2 subunit with a low sensitivity of Mg^{2+} block can be transformed into one with a high sensitivity by exchanging the M1–M4 region. Hence, determinants for subunit specificity of Mg^{2+} block are located within the M1–M4 segment.

Subdividing the M1–M4 region into smaller units resulted in a progressive loss of Mg^{2+} sensitivity. However, three small elements within this region mediated an increase in sensitivity to Mg^{2+} block. These elements are the M1 domain, the small L2 linker connecting M2 and M3, and the M4 domain (see Fig. 3 for definition). Interestingly, NR1-NR2C-M1 and NR1-NR2C-L2 channels exhibited a significant increase in voltage dependence. The NR2C-L2 chimera differs in only four amino acid positions from wild type. Unexpectedly, mutation of any individual amino acid did not result in a change of the $IC_{50,-100mV}$, indicating that a specific set of residues is required to generate this phenotype. Combination of the three elements in chimera NR2C-M1L2M4a resulted in a channel with identical voltage dependence (δ) of block but a slightly different $IC_{50,-100mV}$ compared with NR2B wild type. On the other hand, channels containing NR2C-M14

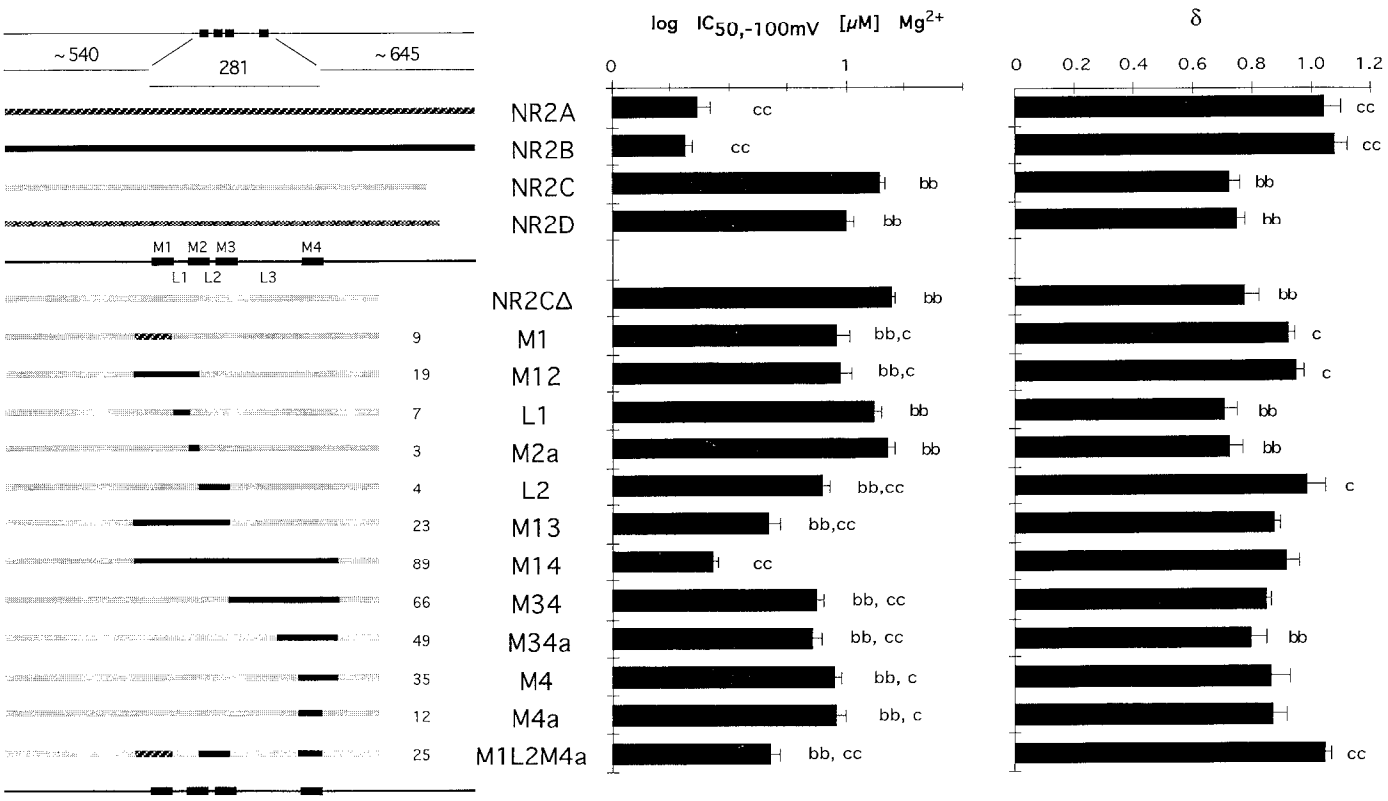

Figure 5. Schematic diagram of wild-type and chimeric subunits. In all subunits, the core region containing M1–M4 is 281 amino acids long and is shown enlarged relative to the N and C termini. *Numbers without units* denote number of amino acids. The *small numbers* next to the schematic representation of the chimeras indicate the number of differing amino acids that are replaced by the given chimera. The *middle panel* shows $\log(IC_{50,-100mV})$ values of Mg^{2+} block; δ is shown on the *right panel*. *Bars* represent mean ± SEMs. Indication of significance levels determined by the Tukey–Kramer test: *c* or *b* = $p < 0.05$, *cc* or *bb* = $p < 0.01$ (comparison to NR2C or NR2B, respectively).

exhibited an $IC_{50,-100mV}$ identical with NR2B wild type and a slightly, but not significantly, decreased value of δ. This discrepancy may reflect limitations of our experimental approach to resolve differences as small as encountered in this case. The three elements contain most of the group-specific differences in amino acid sequence within the M1–M4 segment (see Fig. 3), suggesting that they mediate a group-specific function. We conclude that the M1, L2, and M4 domains are the major structural constituents that mediate subunit-specific differences of Mg^{2+} block in heteromeric NMDAR channels.

Implications for structure and mechanism

Initially, the subunit-specific difference in voltage dependence (δ) suggested that a single site, in addition to the *N-site*, might be sufficient to create subunit specificity of Mg^{2+} block. This can be clearly ruled out by the results shown in this study. Alternatively, four models might be considered for the interpretation of our results in structural terms. Subunit specificity of Mg^{2+} block might be generated by the presence of multiple amino acids at different sites: (1) affecting global properties of the channel (e.g., gating); (2) affecting the positioning of a functionally critical amino acid in the channel (e.g., *N-site*); (3) affecting the interaction of Mg^{2+} with other ions (e.g., Ca^{2+}); (4) interacting directly with Mg^{2+} in the channel (e.g., local changes in surface potential).

Elucidation of the mechanism underlying subunit specificity of Mg^{2+} block may provide evidence favoring one of the models, but it is also conceivable that several mechanisms act in parallel. For example, subunit-specific differences in single-channel properties (Stern et al., 1992) are consistent with model (1). Interpretation of the difference in δ as a difference in location of a site relative to the vertical axis of the channel seems compatible with model (2). Interaction of Mg^{2+} and Ca^{2+} in the channel, which also may account for the deviation from the Woodhull model, sustains model (3). The subunit-specific difference in voltage dependence, interpreted as a difference in local surface potential, favors model (4).

Considering models (3) and (4), it appears relevant that the three elements are putative transmembrane (M1,M4) or membrane-associated (L2) regions, and thus may be located close to the conduction pathway. Functional data (Burnashev et al., 1992), as well as cysteine substitutions (Kuner et al., 1995), indicate that the M2 segment forms at least part of the channel lining. Little is known for the other putative transmembrane segments. Changes in Mg^{2+} block mediated by the M1 segment and RNA editing in the M1 segment of GluR6 (Köhler et al., 1993), in combination with the recently proposed three transmembrane domain (3TM) topology model of glutamate receptors (Hollmann et al., 1994; Wo and Oswald, 1994; Bennett and Dingledine, 1995), indicate that M1 may contribute to the outer vestibule of the channel. Similarly, the L2 loop and parts of M3 might be positioned close to the channel, consistent with the observation that M3 has a modulatory effect on pore structure (Ferrer-Montiel et al., 1995). The 3TM model and results obtained from

cysteine scanning analysis of the M2 segment (Kuner et al., 1995) place the L2 loop on the cytoplasmic side of the membrane. Differences in interaction with ions present at the cytoplasmic channel opening may affect external Mg^{2+} block (Ruppersberg et al., 1994). To date, nothing is known about the positioning of M4 relative to the conduction pathway. It is intriguing to speculate that M4 might contribute to the lining of the channel in conjunction with other transmembrane domains.

In summary, our experiments show that at least three amino acid clusters of the NR2 subunit, likely to be positioned close to the conduction pathway, are required to determine sensitivity of Mg^{2+} block in heteromeric NMDAR channels. The mechanism underlying subunit specificity of Mg^{2+} block remains to be established; however, the models that we provide may guide future studies.

REFERENCES

Akazawa C, Shigemoto R, Bessho Y, Nakanishi S, Mizuno N (1994) Differential expression of five *N*-methyl-D-aspartate receptor subunit mRNAs in the cerebellum of developing and adult rats. J Comp Neurol 347:150–160.

Ascher P, Nowak L (1988) The role of divalent cations in the *N*-methyl-D-aspartate responses of mouse central neurones in culture. J Physiol (Lond) 399:247–266.

Ausubel FM, Brent R, Kingston RE, Moore DD, Seidman JG, Smith JA, Struhl K (1995) Mutagenesis of cloned DNA. In: Current protocols in molecular biology, Chap 8. (Janssen K, ed). New York: Wiley.

Bennett JA, Dingledine R (1995) Topology profile for a glutamate receptor: three transmembrane domains and a channel-lining reentrant membrane loop. Neuron 14:373–384.

Bliss TVP, Collingridge GL (1993) A synaptic model of memory: long-term potentiation in the hippocampus. Nature 361:31–39.

Burnashev N, Schoepfer R, Monyer H, Ruppersberg JP, Günther W, Seeburg PH, Sakmann B (1992) Control by asparagine residues of calcium permeability and magnesium blockade in the NMDA receptor. Science 257:1415–1419.

Burnashev N, Zhou Z, Neher E, Sakmann B (1995) Fractional calcium currents through recombinant GluR channels of the NMDA, AMPA and kainate receptor subtypes. J Physiol (Lond) 485:403–418.

Chen L, Huang L-YM (1992) Protein kinase C reduces Mg^{2+} block of NMDA-receptor channels as a mechanism of modulation. Nature 356:521–523.

Choi DW (1988) Glutamate neurotoxicity and diseases of the nervous system. Neuron 1:623–634.

Collingridge GL, Singer W (1990) Excitatory amino acid receptors and synaptic plasticity. Trends Pharmacol Sci 11:290–296.

Constantine PM (1990) NMDA receptor as a mediator of activity-dependent synaptogenesis in the developing brain. Cold Spring Harb Symp Quant Biol 55:431–443.

DiFrancesco D (1982) Block and activation of the pacemaker channel in calf Purkinje fibres: effects of potassium, caesium and rubidium. J Physiol (Lond) 329:485–507.

Ferrer-Montiel AV, Sun W, Montal M (1995) Molecular design of the *N*-methyl-D-aspartate receptor binding site for phencyclidine and dizolcipine. Proc Natl Acad Sci USA 92:8021–8025.

Hollmann M, Heinemann S (1994) Cloned glutamate receptors. Annu Rev Neurosci 17:31–108.

Hollmann M, Boulter J, Maron C, Beasley L, Sullivan J, Pecht G, Heinemann S (1993) Zinc potentiates agonist-induced currents at certain splice variants of the NMDA receptor. Neuron 10:943–954.

Hollmann M, Maron C, Heinemann S (1994) N-glycosylation site tagging suggests a three transmembrane domain topology for the glutamate receptor GluR1. Neuron 13:1331–1343.

Ikeda K, Nagasawa H, Mori H, Araki K, Sakimura K, Watanabe M, Inoue Y, Mishina M (1992) Cloning and expression of the ε4 subunit of the NMDA receptor channel. FEBS Lett 313:34–38.

Ishii T, Moriyoshi K, Sugihara H, Sakurada K, Kadotani H, Yokoi M, Akazawa C, Shigemoto R, Mizuno N, Masu M, Nakanishi S (1993) Molecular characterization of the family of the *N*-methyl-D-aspartate receptor subunits. J Biol Chem 268:2836–2843.

Jahr CE, Stevens CF (1990) A quantitative description of NMDA receptor-channel kinetic behavior. J Neurosci 10:1830–1837.

Kato N, Yoshimura H (1993) Reduced Mg^{2+} block of *N*-methyl-D-aspartate receptor-mediated synaptic potentials in developing visual cortex. Proc Natl Acad Sci USA 90:7114–7118.

Kato N, Artola A, Singer W (1991) Developmental changes in the susceptibility to long-term potentiation of neurones in rat visual cortex slices. Brain Res Dev Brain Res 60:43–50.

Kawajiri S, Dingledine R (1993) Multiple structural determinants of voltage-dependent magnesium block in recombinant NMDA receptors. Neuropharmacology 32:1203–1211.

Kleckner NW, Dingledine R (1991) Regulation of hippocampal NMDA receptors by magnesium and glycine during development. Brain Res Mol Brain Res 11:151–159.

Köhler M, Burnashev N, Sakmann B, Seeburg PH (1993) Determinants of Ca^{2+} permeability in both TM1 and TM2 of high-affinity kainate receptor channels: diversity by RNA editing. Neuron 10:491–500.

Komuro H, Rakic P (1993) Modulation of neuronal migration by NMDA receptors. Science 260:95–97.

Kuner T, Schoepfer R, Korpi ER (1993) Ethanol inhibits glutamate-induced currents in heteromeric NMDA receptor subtypes. NeuroReport 5:297–300.

Kuner T, Wollmuth LP, Seeburg PH, Sakmann B (1995) Probing the cytoplasmic face of the NMDA receptor channel pore in cysteine-substitution mutants. Soc Neurosci Abstr 21:85.

Kutsuwada T, Kashiwabuchi N, Mori H, Sakimura K, Kushiya E, Araki K, Meguro H, Masaki H, Kumanishi T, Arakawa M, Mishina M (1992) Molecular diversity of the NMDA receptor channel. Nature 358:36–41.

Leonard JP, Kelso SR (1990) Apparent desensitization of NMDA responses in Xenopus oocytes involves calcium-dependent chloride current. Neuron 4:53–60.

Mayer ML, Westbrook GL (1987) Permeation and block of *N*-methyl-D-aspartic acid receptor channels by divalent cations in mouse cultured central neurones. J Physiol (Lond) 394:501–527.

Mayer MS, Westbrook GL, Guthrie PB (1984) Voltage-dependent block by Mg^{2+} of NMDA responses in spinal cord neurones. Nature 309:261–263.

McBain CJ, Mayer ML (1994) *N*-Methyl-D-aspartic acid receptor structure and function. Physiol Rev 74:728–760.

Meguro H, Mori H, Araki K, Kushiya E, Kutsuwada T, Yamazaki M, Kumanishi T, Arakawa M, Sakimura K, Mishina M (1992) Functional characterization of a heteromeric NMDA receptor channel expressed from cloned cDNAs. Nature 357:70–74.

Momiyama A, Feldmeyer D, Cull-Candy SG (1995) Single channel characteristics of NMDA receptors in Purkinje cells in thin slices of neonatal rat cerebellum. J Physiol (Lond) 483.P:163.

Monyer H, Sprengel R, Schoepfer R, Herb A, Higuchi M, Lomeli H, Burnashev N, Sakmann B, Seeburg PH (1992) Heteromeric NMDA receptors: molecular and functional distinction of subtypes. Science 256:1217–1221.

Monyer H, Burnashev N, Laurie DJ, Sakmann B, Seeburg PH (1994) Developmental and regional expression in the rat brain and functional properties of four NMDA receptors. Neuron 12:529–40.

Mori H, Masaki H, Yamakura T, Mishina M (1992) Identification by mutagenesis of a Mg^{2+}-block site of the NMDA receptor channel. Nature 358:673–675.

Moriyoshi K, Masu M, Ishii T, Shigemoto R, Mizuno N, Nakanishi N (1991) Molecular cloning and characterization of the rat NMDA receptor. Nature 354:31–37.

Nabekura J, Kawamoto I, Akaike N (1994) Developmental change in voltage dependency of NMDA receptor-mediated response in nucleus tractus solitarii neurons. Brain Res 648:152–156.

Nowak L, Bregestovsky P, Ascher P, Herbet A, Prochiantz A (1984) Magnesium gates glutamate-activated channels in mouse central neurones. Nature 307:462–465.

Ruppersberg JP, von Kitzing E, Schoepfer R (1994) The mechanism of magnesium block of NMDA receptors. Semin Neurosci 6:87–96.

Sakurada K, Masu M, Nakanishi S (1993) Alteration of Ca^{2+} permeability and sensitivity to Mg^{2+} and channel blockers by a single amino acid substitution in the *N*-methyl-D-aspartate receptor. J Biol Chem 268:410–415.

Sather WA, Yang J, Tsien RW (1994) Structural basis of ion channel permeation and selectivity. Curr Opin Neurobiol 4:313–323.

Schoepfer R, Kuner T, Bche P, Colquhoun D, Stern P (1994) Single channel properties of recombinant NMDA receptors expressed in Xenopus oocytes. Soc Neurosci Abstr 20:309.2.

Seeburg PH, Burnashev N, Köhr G, Kuner T, Sprengel R, Monyer H (1995) The NMDA receptor channel: molecular design of a coincidence detector. Recent Prog Horm Res 50:19–34.

Shatz CJ (1990) Impulse activity and the patterning of connections during CNS development. Neuron 5:745–756.

Stern P, Béhé P, Schoepfer R, Colquhoun D (1992) Single-channel conductances of NMDA receptors expressed from cloned cDNAs: comparison with native receptors. Proc R Soc Lond [Biol] 250:271–277.

Stern-Bach Y, Bettler B, Hartley M, Sheppard PO, O'Hara PJ, Heinemann SF (1994) Agonist selectivity of glutamate receptors is specified by two domains structurally related to bacterial amino acid-binding proteins. Neuron 13:1345–1357.

Watanabe M, Inoue Y, Sakimura K, Mishina M (1992) Developmental changes in distribution of NMDA receptor channel subunit mRNAs. NeuroReport 3:1138–1140.

Wo ZG, Oswald RE (1994) Transmembrane topology of two kainate receptor subunits revealed by N-glycosylation. Proc Natl Acad Sci USA 91:7154–7158.

Woodhull AM (1973) Ionic blockage of sodium channels in nerve. J Gen Physiol 61:687–708.

Yamazaki M, Mori H, Araki K, Mori KJ, Mishina M (1992) Cloning, expression and modulation of a mouse NMDA receptor subunit. FEBS Lett 300:39–45.